

Estimation of Near-Real-Time Outgoing Longwave Radiation from Cross-Track Infrared Sounder (CrIS) Radiance Measurements

KEXIN ZHANG,^a MITCHELL D. GOLDBERG,^b FENGYING SUN,^c LIHANG ZHOU,^d WALTER W. WOLF,^d CHANGYI TAN,^a NICHOLAS R. NALLI,^a AND QUANHUA LIU^d

^a*I. M. Systems Group, Inc., Rockville, Maryland*

^b*NOAA/JPSS, Lanham, Maryland*

^c*Stinger Ghaffarian Technologies, Inc., Greenbelt, Maryland*

^d*NOAA/NESDIS/STAR, College Park, Maryland*

(Manuscript received 22 September 2015, in final form 3 October 2016)


ABSTRACT

This study describes the algorithm for deriving near-real-time outgoing longwave radiation (OLR) from Cross-Track Infrared Sounder (CrIS) hyperspectral infrared sounder radiance measurements. The estimation of OLR on a near-real-time basis provides a unique perspective for studying the variability of Earth's current atmospheric radiation budget. CrIS-derived OLR values are estimated as a weighted linear combination of CrIS-adjusted "pseudochannel" radiances. The algorithm uses the Atmospheric Infrared Sounder (AIRS) as the transfer instrument, and a least squares regression algorithm is applied to generate two sets of regression coefficients. The first set of regression coefficients is derived from collocated Clouds and the Earth's Radiant Energy System (CERES) OLR on *Aqua* and pseudochannel radiances calculated from AIRS radiances. The second set of coefficients is derived to adjust the CrIS pseudochannel radiance to account for the differences in pseudochannel radiances between AIRS and CrIS. The CrIS-derived OLR is then validated by using a limited set of available CERES *SNPP* OLR observations over $1^\circ \times 1^\circ$ global grids, as well as monthly OLR mean and interannual differences against CERES OLR datasets from *SNPP* and *Aqua*. The results show that the bias of global CrIS OLR estimation is within $\pm 2 \text{ W m}^{-2}$ and that the standard deviation is within 5 W m^{-2} for all conditions, and ± 1 and 3 W m^{-2} for homogeneous scenes. The interannual CrIS-derived OLR differences agree well with *Aqua* CERES interannual OLR differences on a $1^\circ \times 1^\circ$ spatial scale, with only a small drift of the global mean of these two datasets of around 0.004 W m^{-2} .

1. Introduction

Long-term measurements of outgoing longwave radiation (OLR) are essential for quantitatively understanding climate in terms of Earth's radiative energy budget within energy balance models (EBMs) and higher-order general circulation models (GCMs) (e.g., Crowley and North 1991). OLR has been widely used as a proxy for tropical convection and precipitation, particularly in diagnosing and understanding tropical intra-seasonal to interannual variability and monsoons (e.g.,

Chelliah and Arkin 1992; Chiodi and Harrison 2010; Xie and Arkin 1996). The trends of OLR have been used to study climate feedbacks and processes (e.g., Chu and Wang 1997; Susskind et al. 2012). Clouds and the Earth's Radiant Energy System (CERES) (Wielicki et al. 1996) was designed to extend the Earth Radiation Budget Experiment (ERBE) data record of TOA longwave (LW) and shortwave (SW) fluxes. Since the infrared (IR) radiance measured in space by radiometers and spectrometers is part of the outgoing LW flux, there have been methods to estimate the OLR by combining radiance observations in several spectral regions. For example, a single IR window channel radiance ($10\text{--}12 \mu\text{m}$) from the Advanced Very High Resolution (AVHRR) was used to estimate the OLR by Ohring et al. (1984). By adding water vapor variance, the two-channel technique was applied to calculate the OLR from the geostationary satellite

 Denotes content that is immediately available upon publication as open access.

Corresponding author e-mail: Kexin Zhang, kexin.zhang@noaa.gov

Meteorological Satellite (Meteosat)-2 by Schmetz and Liu (1988). A multispectral OLR estimation method was developed by Ellingson et al. (1989) using narrowband radiance observations from the High Resolution Infrared Radiation Sounder (HIRS) to estimate TOA total long-wave flux. Vigorous validation efforts were performed for the HIRS multispectral OLR estimation technique against broadband observations derived from the ERBE and the CERES (Ellingson et al. 1994; Lee et al. 2007). These studies have showed that this OLR estimation algorithm can reliably achieve an accuracy of about $4\text{--}8\text{ W m}^{-2}$, with biases that are within the respective radiometric accuracy of the reference instruments.

Beginning in 2002, the Atmospheric Infrared Sounder (AIRS) on board *Aqua* in afternoon (PM) orbit (Aumann et al. 2003) has obtained high-resolution IR spectra, followed by the Infrared Atmospheric Sounding Interferometer (IASI) on board *MetOp-A/MetOp-B* in morning (AM) orbit since 2006/2012 (Diebel et al. 1996) and the Cross-Track Infrared Sounder (CrIS) on board *Suomi-NPP* in PM orbit since 2011 (Goldberg et al. 2013). These combined satellite sounding systems are expected to provide a long-term record of high-resolution radiance spectra. A method for estimating top-of-the-atmosphere (TOA) OLR from AIRS radiance measurements was thus subsequently developed by Sun et al. (2010).¹ In this work we use CERES *Aqua* as an absolute reference for all of our hyperspectral IR OLR products, regardless of whether they are from AIRS, IASI, or CrIS, enabling the creation of consistent and stable OLR records from hyperspectral IR sounders. We therefore use AIRS as a transfer instrument with CERES *Aqua* OLR to estimate OLR from IASI and CrIS on a near-real-time basis; this paper will focus on the algorithm for operational CrIS OLR estimation.

The *SNPP* CrIS is a Fourier transform spectrometer with 1305 IR spectral channels over three wavelength ranges: 3.92–4.64, 5.71–8.26, and 9.14–15.38 μm . CrIS scans a 2200-km swath width ($\pm 50^\circ$ earth angle), with 30 Earth-scene views. Each field of regard (FOR) consists of nine field of views (FOVs), in a 3×3 array of 14-km-diameter spots (nadir spatial resolution). CrIS is designed to provide high-vertical-resolution information on the atmosphere's three-dimensional structure of temperature and water vapor. CERES, a three-channel broadband radiometer, measures both solar-reflected and Earth-emitted radiation from the

TOA to the surface (Wielicki et al. 1996). The CERES instrument has three channels—a shortwave channel (0.3–5 μm) to measure reflected solar radiation, a window channel (8–12 μm) to measure Earth-emitted thermal radiation, and a total channel (0.3–200 μm) to measure all wavelengths of radiation. The first CERES instrument was launched aboard the Tropical Rainfall Measuring Mission (TRMM) satellite in 1997. Currently, CERES flight model 5 (FM5) is carried on the *SNPP* spacecraft and there are five CERES instruments operating on three satellites (FM1 and FM2 on *Terra*, FM3 and FM4 on *Aqua*, and FM5 on *SNPP*). The CERES instrument on *SNPP* will provide continuity for the climate data record of Earth's radiant energy. CERES collects 660 footprints every 6.6 s in two Earth scans operated with back-and-forth scanning. Its footprints are approximately 20 km (24 km for *SNPP* CERES) in diameter at nadir ($1.3^\circ \times 2.6^\circ$ FOV).

The advantage of using hyperspectral infrared observed radiance to estimate CERES-like OLR is to provide near-real-time OLR data (within 2-h latency), while the broadband OLR is not available on a real-time basis. The hyperspectral IR-derived OLR has a number of other uses in seasonal and interannual climate applications, such as detecting strong convection, enhancing tropical monitoring, identifying accurate quantification on Madden-Julian oscillation (MJO) evolution, and improving heat wave detection and quantification. For example, the NOAA/NWS/NCEP/Climate Prediction Center (CPC) operations are now using the hyperspectral OLR product derived from IASI as supplemental information for real-time climate monitoring, and they are now working on utilizing the hyperspectral OLR from CrIS. Compared to the operational near-real-time OLR from AVHRR (on 1° latitude \times 1° longitude), the hyperspectral OLR has a finer spatial resolution better suited to capture convective intensity. It also has the capacity to capture the OLR changes related to moisture variations. Hyperspectral IR sounders have outstanding stability and higher confidence in the accuracy and stability of both datasets can be gained by monitoring the differences between CERES and CrIS over time. Also the method is applied operationally at NOAA to *MetOp-A* and *MetOp-B* IASI measurements. This will provide CERES-like products in the midmorning orbit. There is no follow-on to *Terra* CERES. Furthermore, the CrIS instrument will be on a series of Joint Polar Satellite System (JPSS) satellites providing data continuity to at least 2038. OLR derived from both CrIS and IASI will thus provide long-term records of OLR for monitoring climate.

¹ It should be noted that the method is different from the AIRS Science Team version 5 OLR products (Susskind et al. 2012), which is computed as a function of the AIRS-retrieved geophysical parameters.

2. Methodology

a. Data

Measurement datasets used in training include AIRS and CERES. For regression training relating AIRS radiance to CERES *Aqua* OLR, we use AIRS Level 1b and CERES single-scanner footprint (SSF) measurement datasets. The AIRS Level 1b data (version 5) were obtained from the NASA Goddard Earth Sciences Data and Information Services Center (GES DISC) FTP server.² There are 240 granule files per day, and each granule has 135 cross-track scan lines, with 90 footprints per scan line. The regression relationship between *Aqua* CERES OLR and AIRS was determined by using an ensemble collected from one full day of collocated data for each month in 2006. From that period, 1567 good channels were selected out of 2378 AIRS channels. Each CERES SSF product file contains 1 h of instantaneous CERES data obtained from the Atmospheric Science Data Center (ASDC) at NASA Langley Research Center.³ CERES TOA outgoing longwave fluxes (CERES OLRs) are used in our analysis, which are determined by applying an empirical angular distribution mode to the unfiltered longwave radiances. The angular distribution modes are scene dependent, and CERES uses coincident imager measurements (MODIS for *Aqua* and *Terra*, and VIIRS for *SNPP*) to determine scene types (Loeb et al. 2007). CERES *Aqua* FM3 edition 3A SSF products for the same days as AIRS are used as truth for training and testing regression coefficients. The CERES team has compared FM5 measurements on *SNPP* with those from the CERES instruments on *Terra* and *Aqua* for calibration (Su et al. 2015a,b). In addition, because the *SNPP* imager is different from *Terra* and *Aqua*, the improved CERES next-generation angular directional model (ADM) (Loeb et al. 2005, 2007) is applied to *SNPP*. The uncertainty in fluxes derived from FM5 will be addressed by the CERES team in the future.

b. Algorithm description

The longwave radiation spectrum is the result of the combination of surface thermal emission and atmospheric absorption and thermal emission. Radiances across the spectrum are spectrally correlated; therefore, the variance of the spectrum can, to certain degree, be estimated with radiances sampled at several

TABLE 1. Selection of AIRS and CrIS channels in 17 pseudochannels.

Pseudochannel	Center wavenumber (cm ⁻¹)	Width (cm ⁻¹)	No. of CrIS channels	No. of AIRS channels
1	665.81	32.37	52	124
2	710.79	43.68	70	151
3	757.71	48.35	78	88
4	808.68	38.68	61	52
5	847.70	37.57	60	67
6	885.45	36.66	59	64
7	943.04	60.06	96	77
8	1011.43	69.53	111	107
9	1075.52	38.89	62	45
10	1244.78	55.61	45	80
11	1323.68	78.67	63	119
12	1403.84	78.47	63	121
13	1493.64	66.74	53	83
14	1577.48	72.77	59	77
15	2202.71	42.44	17	42
16	2407.46	30.78	13	29
17	2497.91	103.42	41	94

key frequencies. This forms the basis for narrowband to broadband conversion. To avoid AIRS spectral gaps and “bad” channels, which may have noise-equivalent delta temperature (NEDT) > 2 K at the reference temperature of 250 K, we reduced AIRS and CrIS radiance spectra into a small set of “pseudochannels.” A pseudochannel is an ideal bandpass filter whose spectral response function equals one in the spectral range of the pseudochannel but zero elsewhere. We use 1567 (out of 2378) AIRS channels and 1004 (out of 1305) CrIS channels for the pseudochannels. For each pseudochannel *i*, the spectrally convolved radiance *R* given by

$$R(i, \theta) = \frac{1}{v_{2i} - v_{1i}} \int_{v_{1i}}^{v_{2i}} r(v, \theta) dv, \quad (1)$$

where *i* is the index of the pseudochannel, θ is view angle, v_{1i} and v_{2i} are the spectral bandpass limits of the pseudochannel *i*, $r(v, \theta)$ is the radiance at quasi-monochromatic wavenumber *v*, and θ is the view angle. It is a simple trapezoidal numerical integral of AIRS and CrIS radiance. The center wavenumber (cm⁻¹) and width (cm⁻¹) of the pseudochannels are listed in Table 1. The spectrally convolved radiances calculated in this manner are different between AIRS and CrIS. Reasons for this include the spectral resolution, instrument line shape, and instrument radiometric noise used in the forward model. In real observations, different spatial sampling rates, sizes and shapes of footprints, and observing time differences might also be the reason for the discrepancies. Therefore, for each pseudochannel, the

² ftp://airs11.gesdisc.eosdis.nasa.gov/ftp/data/s4pa/Aqua_AIRS_Level1/.

³ https://eosweb.larc.nasa.gov/HORDERBIN/HTML_Start.cgi.

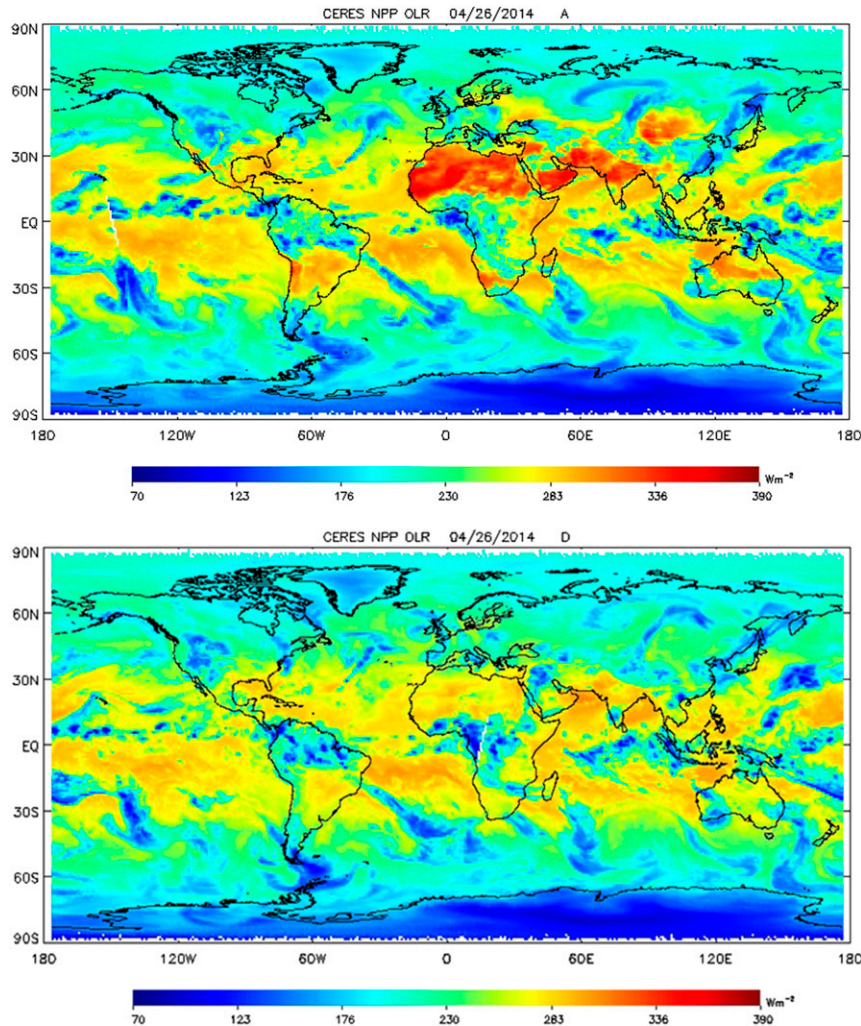


FIG. 1. Outgoing longwave radiation (W m^{-2}) for 26 Apr 2014, derived from the (top) ascending and (bottom) descending orbits of the *SNPP* CERES measurements.

radiance difference ΔR between AIRS and CrIS pseudochannel radiances is adjusted by

$$\Delta R(i) = a_0 + \sum_{k=1}^K a_k r_{\text{CrIS}}(v_k). \quad (2)$$

The regression coefficients a_k are trained by comparing AIRS- and CrIS-simulated radiances using the AIRS and CrIS fast forward radiative transfer algorithms (RTA) by [Strow et al. \(2003\)](#) given “noaa89” sounding collections (7622 sounding profiles representing all-sky conditions). The cloud height and fraction come from [Susskind et al. \(1997\)](#) Pathfinder ATOVS (HIRS + MSU) retrievals that were collocated in time and space. Clouds are assumed as blackbody except for cirrus, which have a spectral-dependent nonunity emissivity. The view angle dependence of radiance is simulated at 90 view angles,

from -49.43° to 49.43° . After deriving the adjustment coefficients in this manner, Eq. (2) is applied to the CrIS-measured radiances in each pseudochannel to generate adjusted pseudochannel radiances. The CrIS OLR is then derived as a linear combination of these adjusted pseudochannel radiances. In the operational NOAA Unique Combined Atmospheric Processing System (NUCAPS) preprocessor the adjustment coefficients and pseudochannel parameters (which include start, end, and center wavenumbers, and a list of CrIS channels and weights) are saved as static ancillary data.

Since the AIRS and CERES instruments are on board EOS *Aqua*, and CrIS and CERES are on *SNPP*, the collocation of AIRS and CERES measurements needs only to be implemented in the spatial domain without considering the observation time difference. [Sun et al. \(2010\)](#) introduced the methodology of the collocation in a

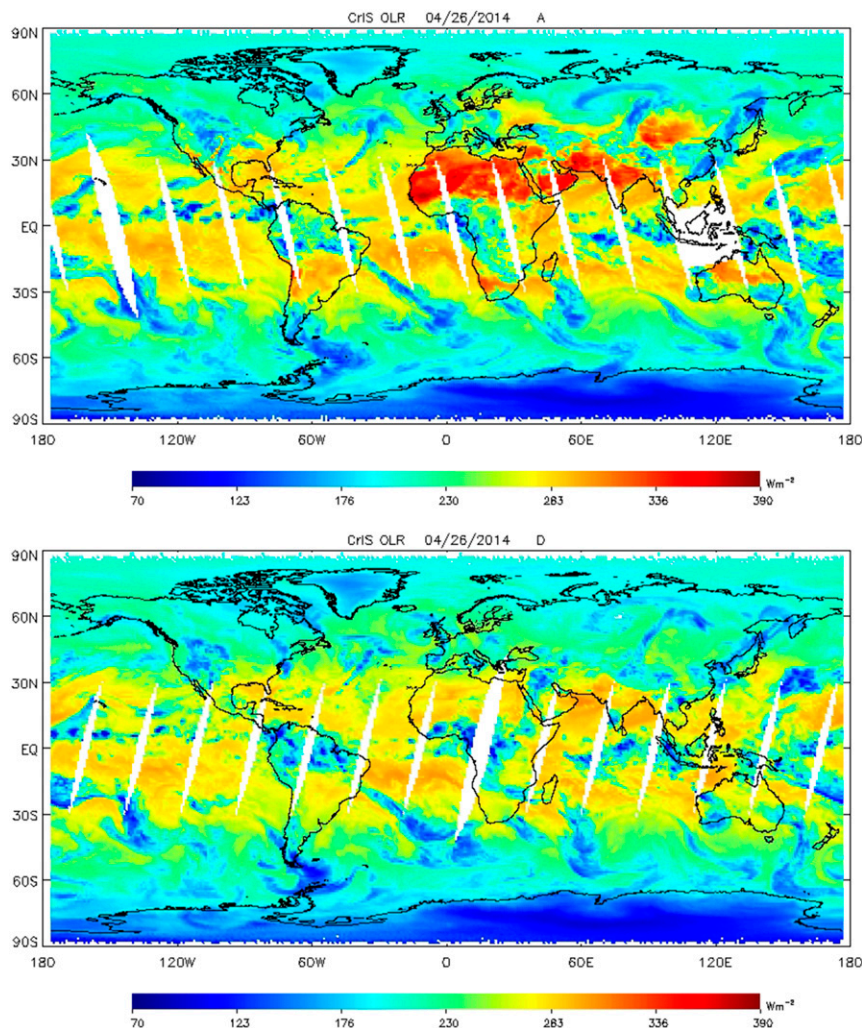


FIG. 2. OLR (W m^{-2}) for 26 Apr 2014, derived from the (top) ascending and (bottom) descending orbits of the CrIS measurements.

“big box,” which includes a 6×5 array of AIRS FOVs. Averaging CERES OLR and AIRS radiances in the big box will minimize the effect of the differences in the view and scanning properties of the two instruments. The coefficient of variation (CV) of CERES OLR in the big box is defined as the ratio of standard deviation divided by the mean. Any box with $\text{CV} \leq 5$ is considered as a uniform scene and is included in the training datasets. The training datasets are selected from one full day each month in 2006 for both AIRS Level 1b and CERES FM3 edition 3A SSF datasets.

The least squares regression algorithm relates the collocated CERES longwave fluxes to AIRS spectrally convolved radiances. The regression coefficients are trained in eight zenith view angle ranges to account for the view angle dependence of AIRS and CrIS radiances. Applying those regression coefficients to adjusted CrIS

spectrally convolved radiances, we get the estimated CrIS OLR in each FOV,

$$\hat{F}_{\text{CrIS}} = b_0(j) + \sum_{i=1}^n b(i,j)[R(i,\theta_j) + \Delta R(i)]; \quad (3)$$

here $n=17$ and j represents one of the eight CrIS viewing angle bins. The 17 pseudochannels are built with the intention to use all of the available information content of both AIRS and CrIS radiance observations. This methodology then allows the estimation of CrIS OLR in each FOV directly from CrIS radiance observations in a simple, robust, and fast way.

3. Results

For validation purposes, we use CrIS sensor data record (SDR) (radiances) and CERES *SNPP* FM5 edition

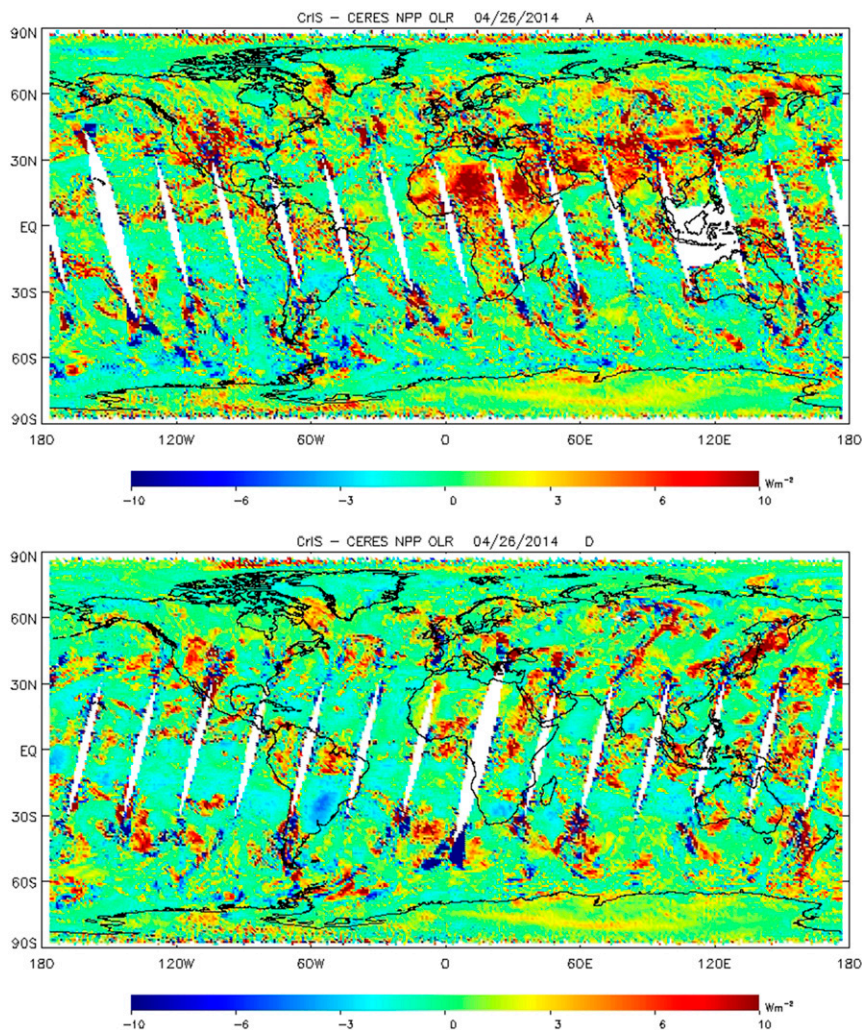


FIG. 3. Differences ($W m^{-2}$) between the CrIS and *SNPP* CERES OLR for the (top) ascending and (bottom) descending orbits of 26 Apr 2014.

1A SSF and CERES *Aqua* FM3 edition 3A datasets. In this paper, we will present the CrIS OLR estimation algorithm using CrIS pseudochannel radiances to predict CERES-like OLR. To validate the accuracy and precision of CrIS-derived CERES-like OLR (CrIS OLR), we use available CERES outgoing longwave radiation fluxes from *SNPP* (*SNPP* CERES OLR) and from *Aqua* (*Aqua* CERES OLR) platforms.

a. Daily OLR

Our operational CrIS OLR will provide near-real-time data daily values with less than 2-h latency, which is more than adequate for weather/climate applications. The daily OLR data can identify the variations in tropical clouds and rainfall that drive global weather patterns. Simultaneous CERES broadband measurements for *SNPP* are the best candidate to validate the CrIS

OLR algorithm. However, the amount of available simultaneous measurement for the study is limited; as of the writing of this paper, *SNPP* CERES OLR SSF products on the NASA ASDC website were available only from 27 January 2012 to 30 June 2014. Also we found the quality flag of the CrIS SDR from the Comprehensive Large Array-Data Stewardship System (CLASS) is suboptimal (too many cases are flagged as bad). We thus requested the NOAA Center for Satellite Applications and Research (STAR) algorithm integration team (AIT) reprocess the CrIS SDRs using the newest version of the offline Algorithm Development Library (ADL) as described by Das et al. (2015).

Because of the difference of the spectral range and spatial resolution of these two instruments, we average CERES and CrIS OLR on a 1° latitude \times 1° longitude grid. Figures 1 and 2 show the $1^\circ \times 1^\circ$ grid *SNPP* CERES

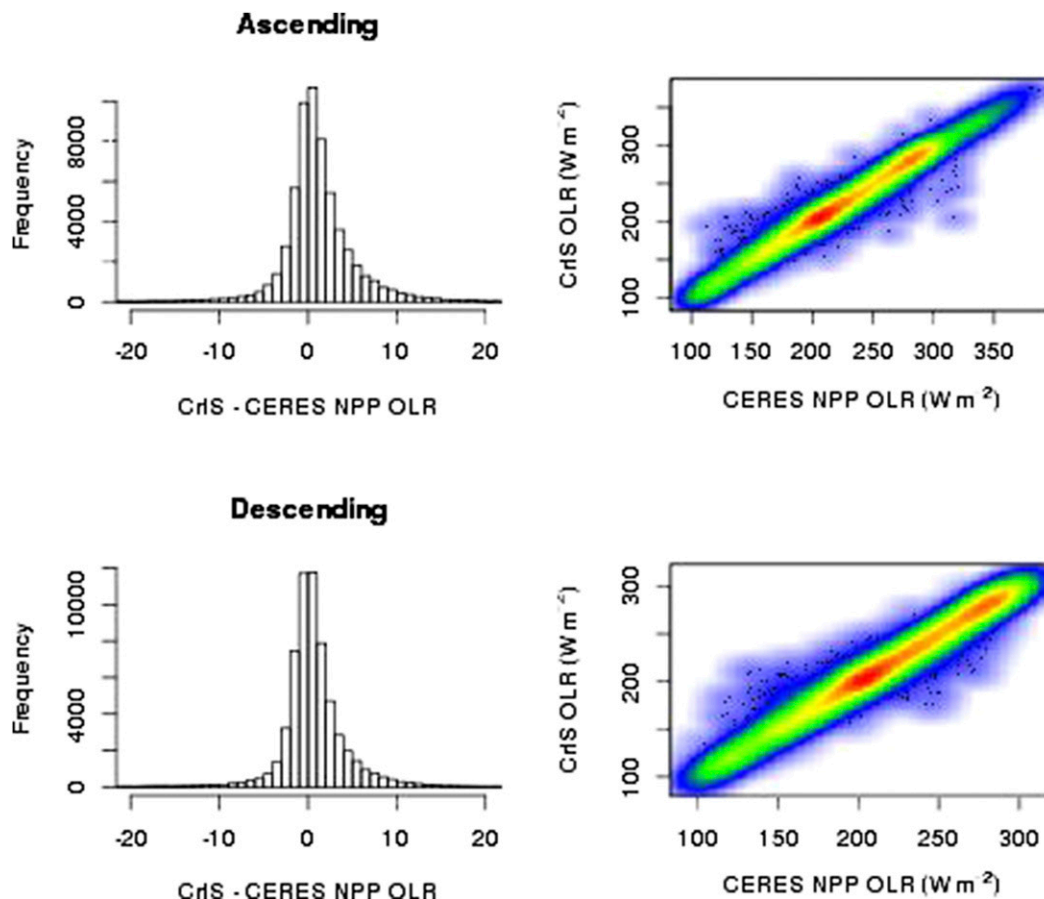


FIG. 4. (left) Histograms of the differences between the *SNPP* CERES OLR and the estimated CrIS OLR for 26 Apr 2014 (right) with scatterplots. Results of OLR for (top) ascending and (bottom) descending orbits. The mean and the standard deviation of the differences between these two OLR datasets are 1.138 and 4.957 W m^{-2} for the ascending orbits and 0.624 and 4.484 W m^{-2} for the descending orbits, respectively.

and CrIS OLR global distribution on 26 April 2014. Both figures agree well, showing geophysically reasonable and spatially consistent patterns. The larger OLR values over major deserts are due to the desert surface emission, and the OLR values near the equator are relatively small due to the high cloud tops associated with the intertropical convergence zone (ITCZ). Note also the large OLR in the vicinity of the oceanic subtropical highs (30°N and 30°S), and Antarctica has the coldest and driest climate, resulting in the lowest OLR. Figure 3 shows the difference distribution corresponding to Figs. 1 and 2. The larger value in bias for the ascending orbits is probably the result of solar radiation during daytime reducing the amount of scene uniformity. Other factors include FOV size and view geometry, both of which can affect apparent cloud cover (Nalli et al. 2012). The large differences occur mostly over land, such as the Sahara Desert region during the daytime, where CrIS OLR presents an overestimation compared with *SNPP* CERES OLR. When we compared the *Aqua* CERES OLR over a $1^{\circ} \times 1^{\circ}$ grid on the same day

(26 April 2014), we found *Aqua* CERES OLR is also overestimated over the Sahara compared with *SNPP* CERES OLR. Recall that CrIS OLR uses *Aqua* CERES OLR as its anchor, so similar patterns such as this might be expected. The NASA CERES team has also reported (W. Su 2016, private communication) on biases between *SNPP* and *Aqua* CERES OLR, and the differences might result from this systematic bias. The differences might also be caused by the different viewing and scanning properties of CrIS and CERES, and inhomogeneous scenes due to the different spatial resolution between these two instruments. In the midlatitudes over convective areas, the cloud amount and cloud-top height might play an important role.

Figure 4 shows the histogram of the differences and the density scatterplot of the estimated CrIS OLR and *SNPP* CERES OLR on 26 April 2014 for both ascending and descending orbits. The bias is near 1 W m^{-2} and the standard deviation is near 5 W m^{-2} . If we remove less homogeneous scenes, which are decided by the

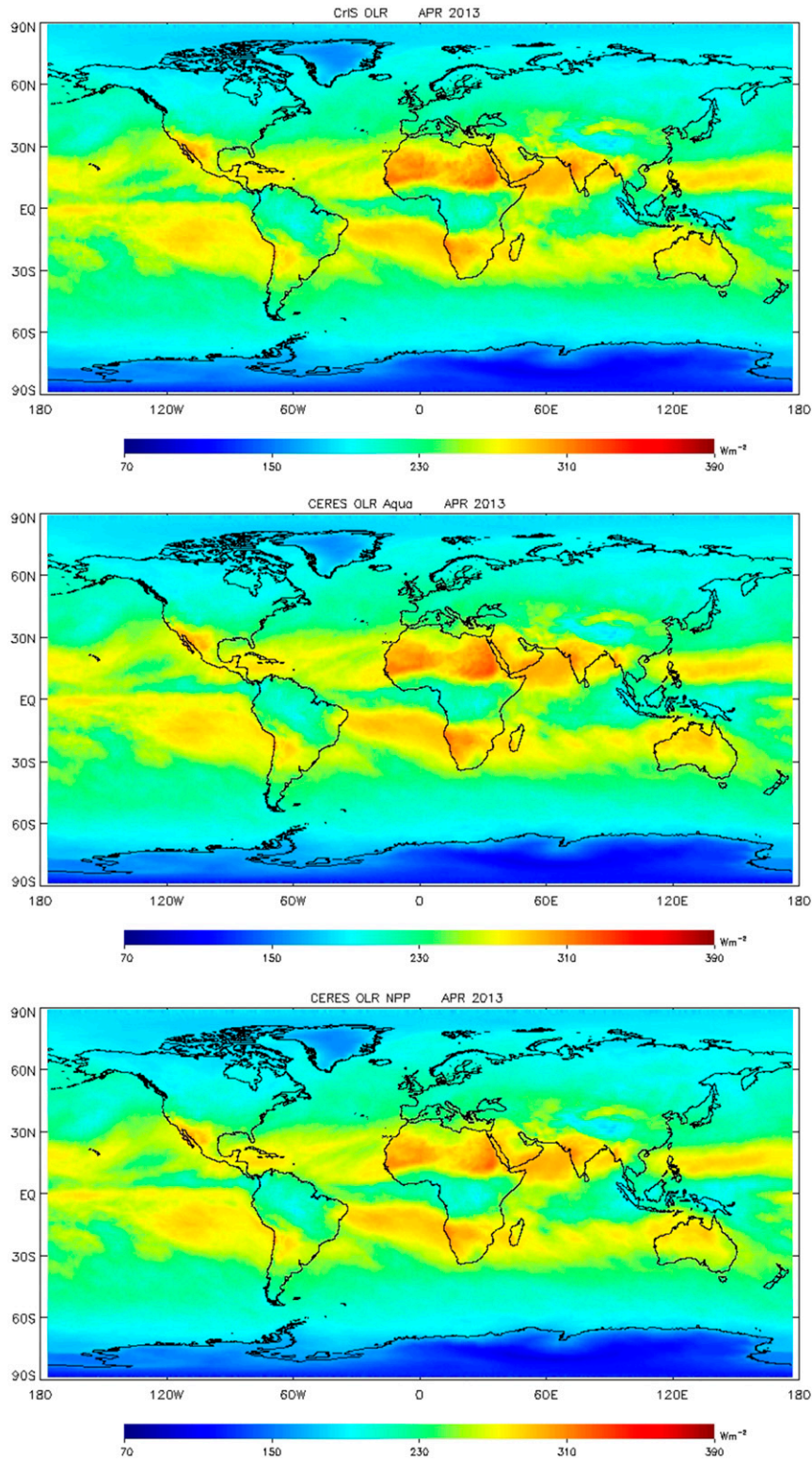


FIG. 5. OLR monthly mean of April 2013 over $1^{\circ} \times 1^{\circ}$ global grids for all scenes: (a) CrIS-derived OLR, (b) *Aqua* CERES OLR, and (c) *SNPP* CERES OLR.

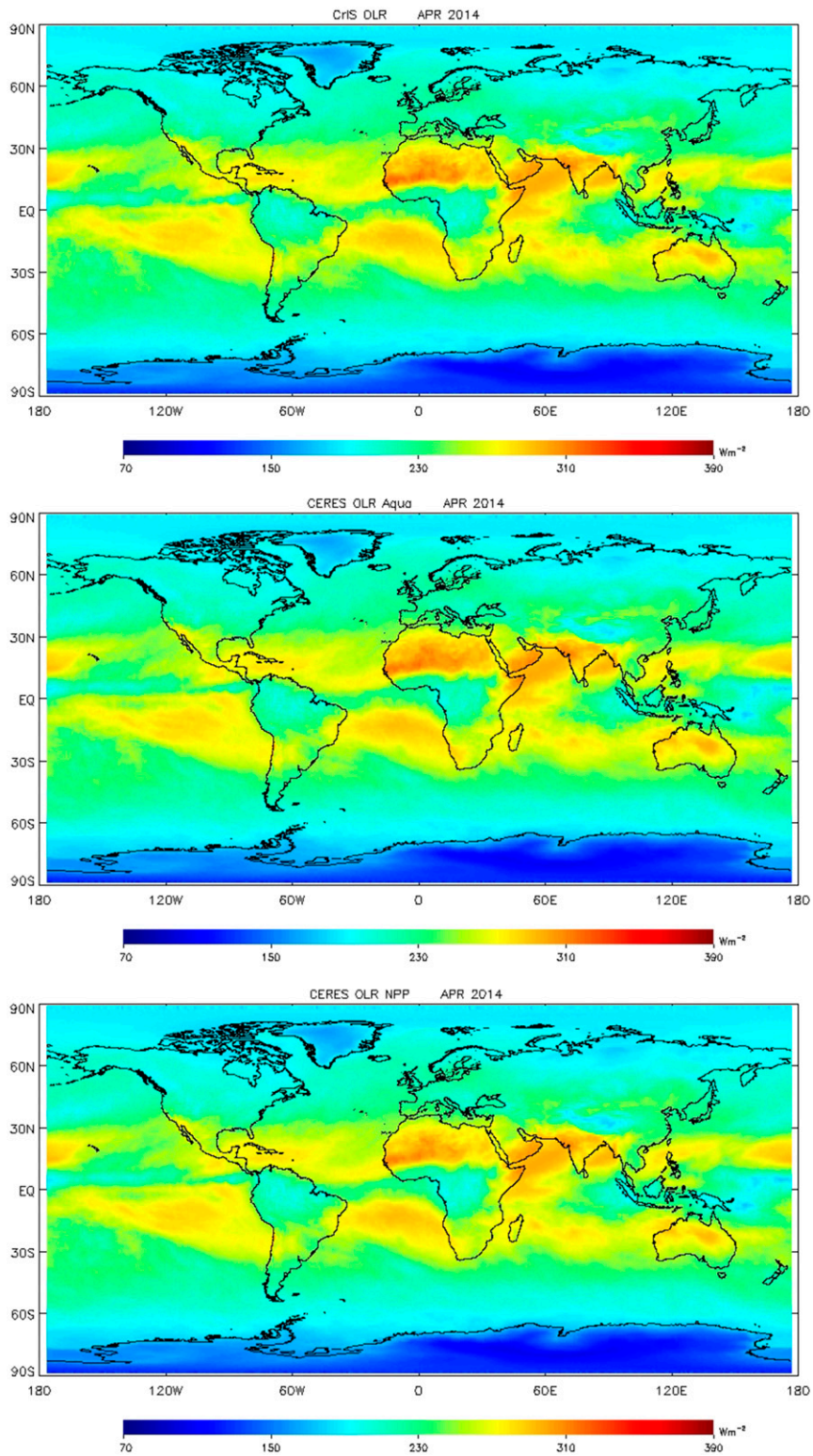


FIG. 6. OLR monthly mean of April 2014 over $1^{\circ} \times 1^{\circ}$ global grids for all scenes: (a) CrIS-derived OLR, (b) *Aqua* CERES OLR, and (c) *SNPP* CERES OLR.

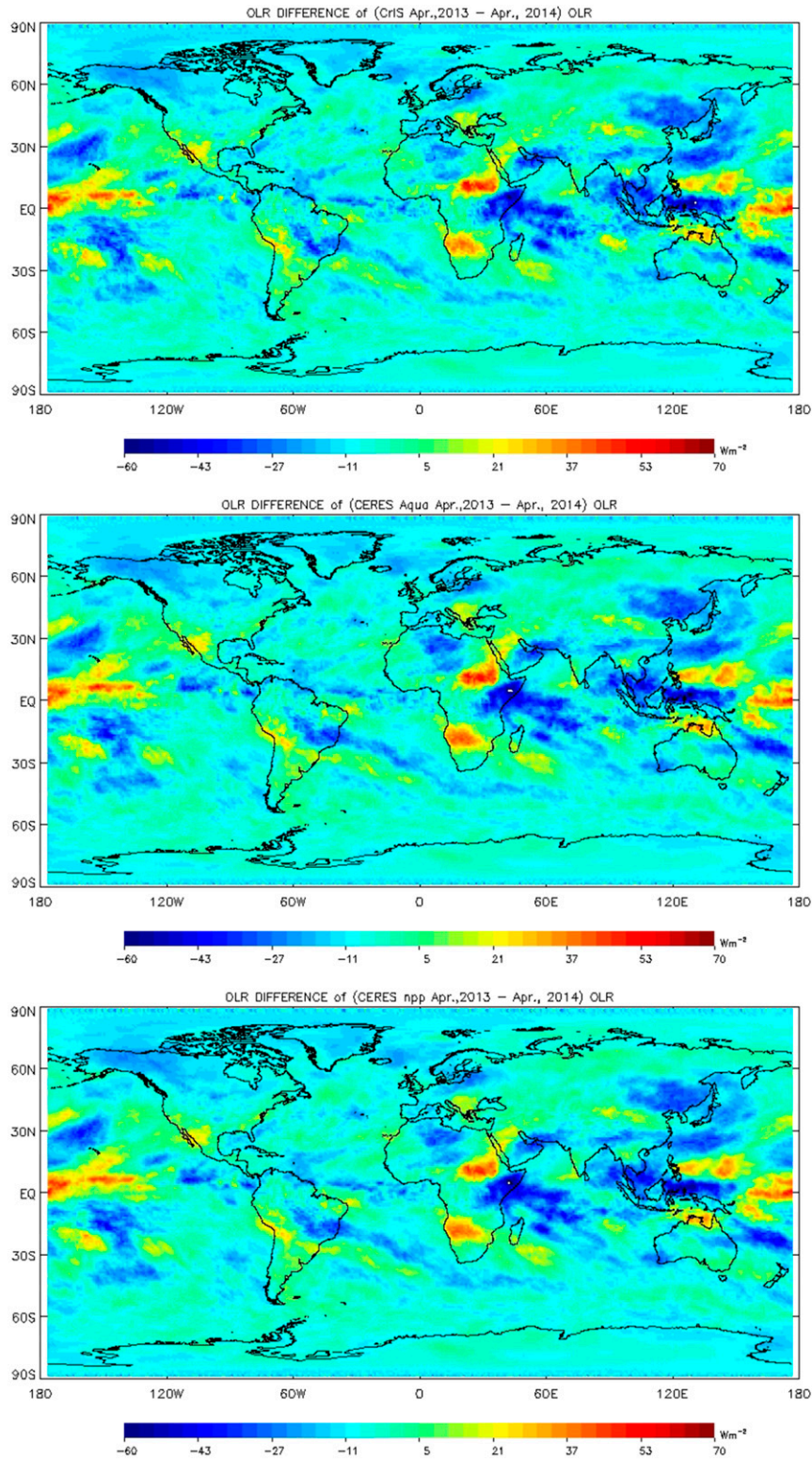


FIG. 7. Interannual OLR differences between April 2013 and April 2014 over $1^\circ \times 1^\circ$ global grids for all scenes: (a) CrIS derived OLR, (b) *Aqua* CERES OLR, and (c) *SNPP* CERES OLR.

TABLE 2. Statistics of OLR monthly mean comparisons for all scenes among CrIS-derived OLR and CERES OLR on *Aqua* and *SNPP*.

Monthly Mean	(CrIS – CERES <i>Aqua</i>) OLR (W m^{-2})			(CrIS – CERES <i>SNPP</i>) OLR (W m^{-2})			(CERES <i>SNPP</i> – <i>Aqua</i>) OLR (W m^{-2})		
	Mean	Std dev	ρ	Mean	Std dev	ρ	Mean	Std dev	ρ
April 2013	–0.1468	2.4732	0.9980	1.2393	2.2704	0.9984	–1.3861	1.9746	0.9988
April 2014	–0.1428	2.3183	0.9980	0.9891	2.0099	0.9985	–1.1319	1.9033	0.9986
Interannual	–0.0040	3.0705	0.9425	0.2501	2.7127	0.955	–0.2541	1.8827	0.9754

threshold of ($\text{CV} \leq 5$) for both *SNPP* CERES and CrIS OLR datasets on each grid point, the bias reduces to less than 1 W m^{-2} and the standard deviation is between 2 and 2.5 W m^{-2} for the uniform scenes, which might be expected from a smaller OLR spatial variation.

b. Monthly mean and interannual variability

Monthly mean fields are important for climate research and were widely used to estimate precipitation by Xie and Arkin (1996). Susskind et al. (2012) compared monthly mean time series of the AIRS version 6 OLR product with those contained in the CERES Energy Balanced and Filled (EBAF) edition 2.6r datasets and showed that the average values of the differences between version 6 OLR and CERES *Terra* OLR, and version 6 OLR_{CLR} and CERES *Terra* OLR_{CLR} are 3.50 and 1.02 W m^{-2} , respectively. Our operational CrIS OLR product uses CrIS radiance measurements as input with static ancillary data to retrieve CERES-like OLR with 2-h latency. It is useful to evaluate CrIS OLR by comparing the monthly mean and interannual variability among those OLR values from different instruments. We generate OLR monthly means on a $1^\circ \times 1^\circ$ global grid by taking the averages of the gridcell values for both ascending and descending orbits each day of a given month for all scenes. Because of the limited CERES *SNPP* OLR datasets available and the missing granules in CrIS SDR datasets, we calculated the monthly means for April 2013 and April 2014 respectively, for *SNPP* CERES, *Aqua* CERES and CrIS-derived OLR, and the global distributions are illustrated in Figs. 5 and 6. The interannual variability (difference between April 2013 and 2014) is shown in Fig. 7, and the ratio between the standard deviation of the OLR interannual differences for CrIS and that of *Aqua* and *SNPP* CERES are 0.998 and 0.993, respectively. The ratios indicate that the OLR interannual variability depicted in the CERES is well captured by the CrIS OLR. The global grid comparisons demonstrate that the spatial patterns agree very well and that the spatial correlation is over 99.8% in monthly mean comparisons. The comparison statistical results are summarized in Table 2. It indicates that there is little drift between CrIS's interannual difference and that of CERES *Aqua*, approximately -0.004 W m^{-2} . The very

small difference of -0.004 is a very important result and can be attributed to the stability of CERES *Aqua*. The training dataset was from 2006 between AIRS and CERES, and these results are from April 2013 and 2014. The CrIS-to-AIRS adjustment [Eq. (2)], which is based on simulated data, introduces no theoretical bias between CrIS and AIRS OLR. Studies by Wang et al. (2012) have shown biases generally within 0.1 K (brightness temperature) between AIRS, CrIS, and IASI with negligible instrument drift. The small bias seen here implies that these hyperspectral infrared sounders provide an effective and highly accurate approach for monitoring OLR. Furthermore, JPSS plans to fly CrIS instruments on a series of JPSS satellites to at least 2038. IASI and the next generation of IASI sensors are slated to operate to at least 2042. OLR from both CrIS and IASI will provide long-term records of OLR for monitoring climate. The interannual variability between CrIS versus *SNPP* CERES and *SNPP* CERES versus *Aqua* CERES is around 0.25 W m^{-2} , which might imply a systematic bias between *Aqua* and *SNPP* CERES OLR.

4. Discussion

This work has demonstrated the ability to estimate OLR using CrIS radiances on a near-real-time basis. CrIS OLR is estimated as weighted linear combination of 17 adjusted CrIS pseudochannel radiances derived using AIRS as a transfer to CERES OLR on *Aqua*. CrIS OLR was compared with simultaneous *SNPP* CERES OLR directly over $1^\circ \times 1^\circ$ global grids. For CrIS scenes, the results show that the standard deviation is near 5 W m^{-2} and that the bias is about 1 W m^{-2} . The spatial correlations of monthly mean between CrIS and CERES *SNPP*, and CrIS and CERES *Aqua* are over 0.998. Future acquired CERES *SNPP* SSF products will be helpful in our algorithm validation, as will regional CrIS OLR analysis, such as the Sahara region. We considered more homogeneous scenes to best represent the performance of the algorithm, since larger discrepancies from the nonuniform scenes are due to the different spatial resolutions between CrIS and CERES. Nevertheless, the algorithm was also seen

to compare reasonably well with CERES for all scenes. For real-time climate monitoring, the algorithm produces results well within 2-h latency. The near-real-time processed CrIS OLR is an ideal candidate for climate applications, and it will enhance the operational climate monitoring, climate analysis, and climate model verification at NOAA's Climate Prediction Center (CPC), which is our primary NOAA user. A series of CrIS instruments are planned for JPSS-1 through JPSS-4 at least to 2038, potentially providing long-term continuity in CrIS OLR for climate monitoring.

Acknowledgments. This study is performed within the project of NOAA Unique Combined Atmospheric System (NUCAPS) funded by the NOAA JPSS program office. The manuscript contents are solely the opinions of the authors and do not constitute a statement of policy, decision, or position on behalf of NOAA or the U.S. government.

REFERENCES

- Aumann, H., and Coauthors, 2003: AIRS/AMSU/HSB on the Aqua mission: Design, science objectives, data products, and processing systems. *IEEE Trans. Geosci. Remote Sens.*, **41**, 253–264, doi:10.1109/TGRS.2002.808356.
- Chelliah, M., and P. Arkin, 1992: Large-scale interannual variability of monthly outgoing longwave radiation anomalies over the global tropics. *J. Climate*, **5**, 371–389, doi:10.1175/1520-0442(1992)005<0371:LSIVOM>2.0.CO;2.
- Chiodi, A. M., and D. E. Harrison, 2010: Characterizing warm-ENSO variability in the equatorial Pacific: An OLR perspective. *J. Climate*, **23**, 2428–2439, doi:10.1175/2009JCLI3030.1.
- Chu, P.-S., and J.-B. Wang, 1997: Recent climate change in the tropical western Pacific and Indian Ocean regions as detected by outgoing longwave radiation records. *J. Climate*, **10**, 636–646, doi:10.1175/1520-0442(1997)010<0636:RCCITT>2.0.CO;2.
- Crowley, T. J., and G. R. North, 1991: *Paleoclimatology*. Oxford University Press, 339 pp.
- Das, B., W. Chen, M. Tsidulko, Y. Zhao, V. Mikles, K. Sprietzer, V. Dharmawardane, and W. Wolf, 2015: Testing, troubleshooting and integrating changes to Joint Polar Satellite Systems (JPSS) algorithms using Algorithm Development Library (ADL). *20th Conf. on Satellite Meteorology and Oceanography*, Phoenix, AZ, Amer. Meteor. Soc., 604. [Available online at http://ams.confex.com/ams/95Annual/webprogram/Handout/Paper260488/AMS2015_BigyaniDas_Poster.pdf.]
- Diebel, D., F. Cayla, and T. Phulpin, 1996: IASI mission rationale, and requirements. Tech. Rep. IASM-0000-10-CNE/EUM, EUMETSAT/CNES/Météo-France, 35 pp.
- Ellingson, R., D. Yanuk, H.-T. Lee, and A. Gruber, 1989: A technique for estimating outgoing longwave radiation from HIRS radiance observations. *J. Atmos. Oceanic Technol.*, **6**, 706–711, doi:10.1175/1520-0426(1989)006<0706:ATFEOL>2.0.CO;2.
- , H.-T. Lee, and D. Yanuk, 1994: Validation of a technique for estimating outgoing longwave radiation from HIRS radiance observations. *J. Atmos. Oceanic Technol.*, **11**, 357–365, doi:10.1175/1520-0426(1994)011<0357:VOATFE>2.0.CO;2.
- Goldberg, M. D., H. Kilcoyne, H. Cikanek, and A. Mehta, 2013: Joint Polar Satellite System: The United States next generation civilian polar-orbiting environmental satellite system. *J. Geophys. Res. Atmos.*, **118**, 13 463–13 475, doi:10.1002/2013JD020389.
- Lee, H.-T., A. Gruber, R. Ellingson, and I. Laszlo, 2007: Development of the HIRS outgoing longwave radiation climate dataset. *J. Atmos. Oceanic Technol.*, **24**, 2029–2047, doi:10.1175/2007JTECHA989.1.
- Loeb, N. G., S. Kato, K. Loukachine, and N. Manalo-Smith, 2005: Angular distribution models for top-of-atmosphere radiative flux estimation from the Clouds and the Earth's Radiant Energy System (CERES) instrument on the Terra satellite. Part I: Methodology. *J. Atmos. Oceanic Technol.*, **22**, 338–351, doi:10.1175/JTECH1712.1.
- , —, —, —, and D. R. Doelling, 2007: Angular distribution models for top-of-atmosphere radiative flux estimation from the Clouds and the Earth's Radiant Energy System (CERES) instrument on the Terra satellite. Part II: Validation. *J. Atmos. Oceanic Technol.*, **24**, 564–584, doi:10.1175/JTECH1983.1.
- Nalli, N. R., C. D. Barnet, E. S. Maddy, and A. Gambacorta, 2012: On the angular effect of residual clouds and aerosols in clear-sky infrared window radiance observations: Sensitivity analyses. *J. Geophys. Res.*, **117**, D12208, doi:10.1029/2012JD017667.
- Ohring, G., A. Gruber, and R. Ellingson, 1984: Satellite determinations of the relationship between total longwave radiation flux and infrared window radiance. *J. Climate Appl. Meteor.*, **23**, 416–425, doi:10.1175/1520-0450(1984)023<0416:SDOTRB>2.0.CO;2.
- Schmetz, J., and Q. Liu, 1988: Outgoing longwave radiation and its diurnal variation at regional scales derived from Meteosat. *J. Geophys. Res.*, **93**, 11 192–11 204, doi:10.1029/JD093iD09p11192.
- Strow, L., S. Hannon, S. DeSouza-Machado, D. Tobin, and H. Motteler, 2003: An overview of the AIRS radiative transfer model. *IEEE Trans. Geosci. Remote Sens.*, **41**, 303–313, doi:10.1109/TGRS.2002.808244.
- Su, W., J. Corbett, Z. Eitzen, and L. Liang, 2015a: Next-generation angular distribution models for top-of-atmosphere radiative flux calculation from the CERES instruments: Methodology. *Atmos. Meas. Tech.*, **8**, 611–632, doi:10.5194/amt-8-611-2015.
- , —, —, and —, 2015b: Next-generation angular distribution models for top-of-atmosphere radiative flux calculation from the CERES instruments: Validation. *Atmos. Meas. Tech.*, **8**, 4489–4536, doi:10.5194/amt-8-4489-2015.
- Sun, F., M. Goldberg, X. Liu, and J. Bates, 2010: Estimation of outgoing longwave radiation from Atmospheric Infrared Sounder radiance measurements. *J. Geophys. Res.*, **115**, D09103, doi:10.1029/2009JD012799.
- Susskind, J., P. Piraino, L. Rokke, L. Iredell, and A. Mehta, 1997: Characteristics of the TOVS Pathfinder Path A dataset. *Bull. Amer. Meteor. Soc.*, **78**, 1449–1472, doi:10.1175/1520-0477(1997)078<1449:COTTPP>2.0.CO;2.
- , G. Molnar, L. Iredell, and N. Loeb, 2012: Interannual variability of outgoing longwave radiation as observed by AIRS and CERES. *J. Geophys. Res.*, **117**, D23107, doi:10.1029/2012JD017997.

- Wang, L., Y. Han, D. Tremblay, F. Weng, and M. Goldberg, 2012: Intercomparison of NPP/CrIS radiances with VIIRS, AIRS, and IASI: A post-launch calibration assessment. *Earth Observing Missions and Sensors: Development, Implementation, and Characterization II*, H. Shimoda et al., Eds., International Society for Optical Engineering (SPIE Proceedings, Vol. 8528), 85280J, doi:[10.1117/12.978769](https://doi.org/10.1117/12.978769).
- Wielicki, B. A., B. R. Barkstrom, E. F. Harrison, R. B. Lee, G. L. Smith, and J. E. Cooper, 1996: Clouds and the Earth's Radiant Energy System (CERES): An earth observing system experiment. *Bull. Amer. Meteor. Soc.*, **77**, 853–868, doi:[10.1175/1520-0477\(1996\)077<0853:CATERE>2.0.CO;2](https://doi.org/10.1175/1520-0477(1996)077<0853:CATERE>2.0.CO;2).
- Xie, P., and P. Arkin, 1996: Analyses of global monthly precipitation using gauge observations, satellite estimates, and numerical model predictions. *J. Climate*, **9**, 840–858, doi:[10.1175/1520-0442\(1996\)009<0840:AOGMPU>2.0.CO;2](https://doi.org/10.1175/1520-0442(1996)009<0840:AOGMPU>2.0.CO;2).